How to cite: *Angew. Chem. Int. Ed.* **2020**, *59*, 20215–20223
International Edition: doi.org/10.1002/anie.202010169
German Edition: doi.org/10.1002/ange.202010169

Imaging

Descriptor $\Delta G_{C\text{-}O}$ Enables the Quantitative Design of Spontaneously Blinking Rhodamines for Live-Cell Super-Resolution Imaging

Weijie Chi[+], Qinglong Qiao[+], Chao Wang, Jiazhu Zheng, Wei Zhou, Ning Xu, Xia Wu, Xiao Jiang, Davin Tan, Zhaochao Xu, and Xiaogang Liu**

Abstract: *Herein, we reported a simple, fast, and quantitative theoretical descriptor $\Delta G_{C\text{-}O}$ that allows accurate predictions of a wide range of spontaneously blinking rhodamines. $\Delta G_{C\text{-}O}$ denotes the Gibbs free energy differences between the closed and open forms of rhodamines and has a good linear relationship with experimental pK_{cycl} values. This correlation affords an effective guide for the quantitative designs of spontaneously blinking rhodamines and eliminates trial-and-error. We have validated the predictive power of $\Delta G_{C\text{-}O}$ via the development of two spontaneously blinking rhodamines of different colors and enhanced brightness. We also demonstrated their super-resolution imaging utilities in dynamic live-cell imaging. We expect that $\Delta G_{C\text{-}O}$ will greatly facilitate the efficient creations of spontaneously blinking fluorophores and aid the advancements of super-resolution bioimaging techniques.*

Introduction

Single-molecule localization microscopy (SMLM) breaks the diffraction limit and provides unprecedented spatial resolution through the temporal separation of adjacent fluorescent fluorophores via the switching of dark and fluorescent pair states.[1] However, intense laser irradiations or additives required for inducing the blinking of photoactivable or photoswitchable fluorophores limit the application of SMLM in live-cell imaging.[1b,c] In contrast, fluorescent dyes that spontaneously blink via thermal equilibrium greatly improve the biocompatibility of SMLM imaging, simplify the imaging treatment and equipment, and allow long time-lapse live-cell super-resolution imaging.[2] To date, such optimal spontaneously blinking fluorophores are in great demand but still sorely lacking; more critically, the development of these fluorophores remains slow, posing a major bottleneck for the rapid evolution of the SMLM technologies.[3] It is thus imperative to bring new design approaches into the field of dye chemistry, to facilitate the efficient and effective creations of high-performance SMLM fluorophores.

Among various fluorophores, rhodamine dyes are the most gifted class of dyes for a wide range of applications, owing to their outstanding photophysical properties and biocompatibility.[4] Notably, rhodamines possess a reversible spirocyclization reaction, switching between the closed form (non-emissive, lipophilic and colorless) and the open form (fluorescent and colored). This spirocyclization equilibrium can be adjusted via various chemical substitutions on the xanthene scaffold (such as at X, Y, and R) and described by several parameters (such as $\Delta G_{C\text{-}O}$ and pK_{cycl}; Figure 1 a).[2b,5] Depending on this equilibrium, sparse emissions and the blinking of rhodamines for super-resolution imaging can be

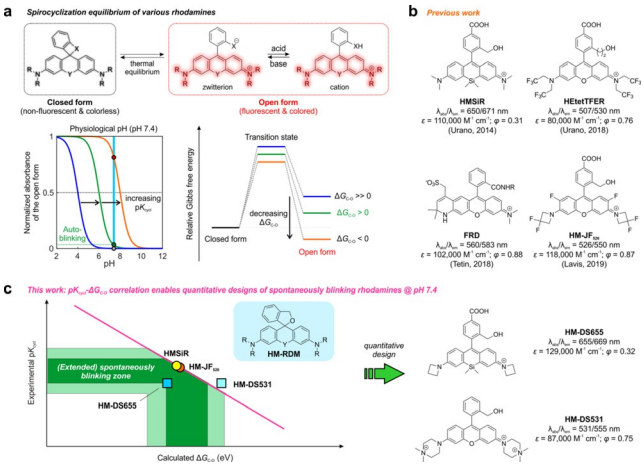

Figure 1. a) Illustration of spirocyclization equilibrium between the closed form and the open form of rhodamines, and photophysical parameters that reflect this equilibrium (such as $\Delta G_{C\text{-}O}$ and pK_{cycl}). b) Molecular structures and photophysical properties of spontaneously blinking rhodamines previously reported; λ_{abs}, peak UV/Vis absorption wavelength; λ_{em}, peak emission wavelength; ε, molar extinction coefficient; φ, quantum yield. c) Illustration of the correlation between calculated $\Delta G_{C\text{-}O}$ and experimental pK_{cycl} values for a series of reported hydroxymethyl rhodamine dyes, and new spontaneously blinking rhodamines developed with the guidance of this correlation.

[*] Dr. W. Chi,[+] Dr. Q. Qiao,[+] Dr. C. Wang, J. Zheng, W. Zhou, N. Xu, Prof. Dr. Z. Xu
CAS Key Laboratory of Separation Science for Analytical Chemistry, Dalian Institute of Chemical Physics, Chinese Academy of Sciences
457 Zhongshan Road, Dalian 116023 (China)
E-mail: zcxu@dicp.ac.cn
Dr. W. Chi,[+] Dr. C. Wang, X. Wu, Dr. D. Tan, Prof. Dr. X. Liu
Fluorescence Research Group
Singapore University of Technology and Design
8 Somapah Road, 487372, Singapore (Singapore)
E-mail: xiaogang_liu@sutd.edu.sg
Dr. X. Jiang
Key Laboratory of Industrial Ecology and Environmental Engineering (MOE), School of Environmental Science and Technology
Dalian University of Technology
Linggong Road 2, Dalian 116024 (China)
[+] These authors contributed equally to this work.
Supporting information and the ORCID identification number(s) for the author(s) of this article can be found under: https://doi.org/10.1002/anie.202010169.

achieved in three ways (Supporting Information, Figure S1). In the first method (photobleaching and imaging), when most rhodamines are in the fluorescent open form, an intense visible laser is required to bleach these fluorophores into non-emissive triplet states or other dark states, followed by stochastic transitions to the bright states for imaging (Supporting Information, Figure S1a).[6] In the second method (photoactivation and imaging), when (almost) no rhodamines are in the open form, additional UV or blue photoactivation light is required to promote the ring-opening reactions and enable random and spare emissions, before the bright fluorophores return to the dark states either via spirocyclization or photobleaching (Supporting Information, Figure S1b).[7] Unfortunately, in both methods, intense photobleaching laser and/or the short wavelength photoactivation laser not only complicate the optical setup (with high cost), but also introduce serious phototoxicity and influence cellular physiology for live-cell imaging. Moreover, the effective blinking of those fluorophores often demands tedious tuning of imaging buffer conditions. In contrast to these two methods, the third one (direct imaging) is much more favorable, in which a small number of rhodamines are in the fluorescent open form, sparsely emits, and spontaneously blink due to the thermal equilibrium between its open and closed forms in the ground state (Supporting Information, Figure S1c).[2b,8] The spontaneously blinking rhodamines afford significant advantages: 1) they do not require photobleaching and photoactivation laser, greatly reducing phototoxicity and enabling efficient use of photon budget for long time-lapse imaging; 2) they require neither additives nor imaging buffer optimizations, and permits cellular imaging under physiological conditions; 3) it greatly simplifies the optical setup of SMLM, such that super-resolution imaging can be (in principle) performed on standard microscopies that are already available in most biological labs.

In a landmark study conducted in 2014, the Urano group reported a milestone development of the first-of-kind spontaneously blinking Si-rhodamine dye **HMSiR** (Figure 1b).[2b] They noted that the blinking performances of rhodamines were correlated to the energy of the lowest unoccupied molecular orbitals of xanthene moieties ($r^2 = 0.630$).[2b] The same group also introduced the first green spontaneously blinking dye **HEtetTFER** in 2018 (Figure 1b).[9] Collectively, these two dyes enabled the dual-color SMLM in an additive-free buffer solution. However, the brightness of both **HMSiR** and **HEtetTFER** remains sub-optimal, and the latter is not suitable for live-cell imaging.[10] Consecutively, Tetin et al. reported a yellow spontaneously blinking dye **FRD** in 2018 (Figure 1b).[11] Unfortunately, the rate of blinking is slow (on the order of seconds to minutes) for **FRD**, limiting its application in dynamic imaging. In 2019, the Lavis group established a quantitative $K_{L\text{-}Z}$ framework for the development of fluorogenic and spontaneously blinking rhodamines, based on which one yellow spontaneously blinking fluorophore **HM-JF$_{526}$** was developed (Figure 1b).[12] Nevertheless, without prior synthesis, it is difficult to quantitatively predict $K_{L\text{-}Z}$ of new rhodamines, since X, Y, R and other groups on the xanthene scaffold collectively determine the value of $K_{L\text{-}Z}$. Furthermore, only a small subset of individual fluorophores is allowed to be in the Fluorescence-On state at physiological pH for single-molecule localization. As the ratio of the open form population in rhodamines spans from 0 to 1, this ratio corresponding to the spontaneously blinking rhodamines is on the order of only one percent (Figure 1a). Consequently, shifting the spirocyclization equilibrium into this extremely narrow spontaneously blinking window requires sophisticated tuning and laborious trial-and-error via the synthesis and screening of many derivatives (Figure 1c). These demanding requirements seriously hinder the development of spontaneously blinking rhodamines for SMLM imaging. An improvement in the development protocol towards quantitative and precise designs is thus undoubtedly necessary.

Herein, inspired by the ground-breaking work of experimentalists and based on our previous work on the ring-opening mechanism of rhodamines,[5] we reported a simple, fast and quantitative descriptor $\Delta G_{C\text{-}O}$ [the change of Gibbs free energy from the closed form to the open form (Figure 1c); the open form is represented by the zwitterion] for accurately predicting spontaneously blinking rhodamine dyes. We show that $\Delta G_{C\text{-}O}$ between 1.156 and 1.248 eV is a good indicator of developing spontaneously blinking hydroxymethyl rhodamines at physiological pH (7.4). Guided by $\Delta G_{C\text{-}O}$, we have computationally designed five and experimentally validated two spontaneously blinking hydroxymethyl rhodamine dyes with improved brightness for SMLM imaging (Figure 1c). We expect that our method will significantly facilitate the effective creation of multi-colored spontaneously blinking dyes, and greatly aid the development of super-resolution imaging in live cells.

Results and Discussion

Establishing a $\Delta G_{C\text{-}O}$-pK_{cycl} Based Prediction Model of Spontaneously Blinking Rhodamines

Since the sparse emissions and spontaneous blinking of rhodamines are governed by the thermal equilibrium between their open and closed forms in the ground state, the Gibbs free energy difference between the closed and open forms ($\Delta G_{C\text{-}O}$) would serve as a useful descriptor for predicting spontaneously blinking rhodamine dyes (Figure 1a).[5] When $\Delta G_{C\text{-}O}$ becomes higher, a lower percentage of rhodamines are in the fluorescent open form. Hence, a slightly positive $\Delta G_{C\text{-}O}$ is essential to ensure that sparse but sufficient rhodamines are in the open form, while the thermal spirocyclization equilibrium randomly and reversibly switches rhodamines on/off and induces blinking.

Although it is experimentally difficult to measure $\Delta G_{C\text{-}O}$, this parameter can be easily calculated via density functional theory calculations.[5]

Besides $\Delta G_{C\text{-}O}$, the spirocyclization equilibria of rhodamines are also reflected by pK_{cycl} (Figure 1a). Herein pK_{cycl} is the pH value at which the absorbance of rhodamine decreases to half of its maximum due to spirocyclization; a lager pK_{cycl} value indicates that more rhodamines stay in the open form within the cellular environment (ca. pH $\approx$ 7.4).[13]

pK_{cycl} values can be easily measured via experiments, and have been widely reported in the literature.[2b,9,13,14]

Given that both calculated $\Delta G_{C\text{-}O}$ and experimental pK_{cycl} reflect the population of open form rhodamines, we hypothesized that a correlation between these two parameters existed, and this correlation would facilitate quantitative prediction of the open-form rhodamine populations, and thereby enable the computational design of spontaneously blinking rhodamines (with sparse emissions).

To verify our hypothesis, we collected the pK_{cycl} values of 25 existing hydroxymethyl rhodamine dyes reported by the Urano group (**U1**–**U25** in the Supporting Information, Figure S2).[2b,14a,b] We also calculated their $\Delta G_{C\text{-}O}$ values at M06-2X/TZVP level and the SMD solvent model (in water)[15] (Supporting Information, Section 1; Figures S3–S27, and Table S1). Previous reports have also validated the reliability of the M06-2X functional in studying the geometric structures and Gibbs free energies of organic molecules.[15a,16] During these calculations (Figure 2a), we used zwitterions to represent the open forms. To our delight, we discovered an excellent linear correlation ($r^2 = 0.965$) between calculated $\Delta G_{C\text{-}O}$ and experimental pK_{cycl} values (Figure 2b). This correlation allows us to reliably predict pK_{cycl} values of rhodamines via simple ground-state calculations. The mean absolute error of our pK_{cycl} predictions is only 0.30 (Supporting Information, Figure S31 and Table S1); the standard deviation of these absolute errors amounts to about 0.21.

To affirm the reliability of this correlation, we further predicted the pK_{cycl} values of **U26**–**U28**, three recent rhodamines reported by the Urano group (Supporting Information, Figures S28–S30 and Table S1).[9,14c] Our predicted pK_{cycl} values of **U26**–**U28** are very close to experimental data, with absolute errors of about 0.33. These results demonstrate the outstanding predictive power of $\Delta G_{C\text{-}O}$.

For the calculations of $\Delta G_{C\text{-}O}$, we also considered cations representing the open forms of **U1**–**U25**. This treatment leads to a good linear correlation with pK_{cycl} as well ($r^2 = 0.951$; Figure 2b; Supporting Information, Table S2). Moreover, we inserted explicit molecules near the hydroxymethyl group of **U1**–**U25** to account for specific solvent effects, and recalculated $\Delta G_{C\text{-}O}$ (Supporting Information, Figures S32–S37 and Table S3). The molecular electrostatic potential surface (Figure 2b inset) and the Gibbs free energy of the rhodamine and water complex affirmed that the hydroxymethyl group was prone to hydrogen bond interactions (Supporting Information, Figure S32). Indeed, the interaction energy between rhodamine and water of **U7-O-W** (around the hydroxymethyl group; 0.214 eV) is larger than that of **U7-N-W** (around the dimethylamino group; 0.173 eV; Supporting Information, Figure S32). The resulting linear correlation with pK_{cycl} remains good ($r^2 = 0.922$; Figure 2b). These results suggest that the effect of pH and solvent effect on $\Delta G_{C\text{-}O}$ can be accounted for by a (nearly) constant offset for structurally similar rhodamines; the negligence of these factors does not deteriorate the predictive power of calculated $\Delta G_{C\text{-}O}$ for pK_{cycl}. We thus chose the computational results using zwitterions to represent the open forms and without explicit solvent molecules for simplicity in subsequent analysis. It is also interesting to note a good linear correlation between $\Delta G_{C\text{-}TS}$ and pK_{cycl} ($r^2 = 0.9184$; Supporting Information, Figure S38 and Table S4).

Notably, Urano has proposed that a pK_{cycl} value of ≤ 6.0 was a good indicator to ensure sparse emissions of hydroxymethyl rhodamines in biological cells.[2b] However, as pK_{cycl} continues to decrease, the population of the open form rhodamines keeps dropping, and the open form lifetime in the ground state also reduces. Based on the reported experimental data,[2b] we further proposed a pK_{cycl} value of ≥ 5.3 as the lower threshold value for spontaneously blinking hydroxymethyl rhodamine dyes in a nearly neutral cellular environment (Supporting Information, Figure S39, Tables S5 and S6). This lower threshold serves two purposes: 1) ensure an adequate lifetime of the open form rhodamines in the ground state, which synchronizes with imaging acquisition speed for collecting ample photons and improving imaging resolution (on the order of 10 to 100 ms); 2) provide a sufficient population of the open form rhodamines; that is, sparse, but not too sparse.

Moreover, given the average error of 0.3 in the computational prediction of pK_{cycl} values, we decided to extend the

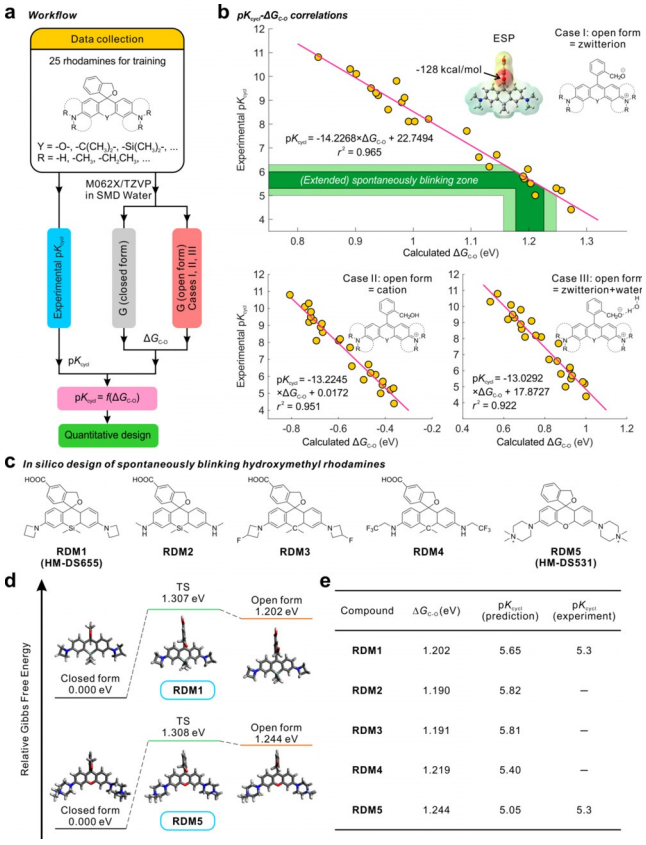

Figure 2. a) Our workflow in this work. b) Correlations between calculated $\Delta G_{C\text{-}O}$ and experimental pK_{cycl} values for a series of hydroxymethyl rhodamine dyes reported by the Urano group; during our calculations, we considered three types of open forms: zwitterion, cation, and zwitterion + water. c) Molecular structures of computationally designed spontaneously blinking rhodamines **RDM1**-**RDM5**. d) Optimized molecular structures and calculated relative Gibbs free energies of **RDM1** and **RDM5** in water. e) Calculated $\Delta G_{C\text{-}O}$, predicted pK_{cycl}, and experimental pK_{cycl} values of **RDM1**-**RDM5** in water.

permissible pK_{cycl} range from [5.3, 6.0] (experimental) to [5.0, 6.3] (calculated), to capture more potential spontaneously blinking rhodamines during computational predictions. Based on the $\Delta G_{C\text{-}O}$-pK_{cycl} correlation, the extended pK_{cycl} range of [5.0, 6.3] translates to the $\Delta G_{C\text{-}O}$ value of [1.156, 1.248 eV]. Consequently, one can rapidly design calculated spontaneously blinking rhodamines, by conducting simple ground-state calculations and ensuring that the resulted $\Delta G_{C\text{-}O}$ values fall into this desirable range.

Computational Design of Spontaneously Blinking Hydroxymethyl Rhodamine Dyes

Inspired by the success of $\Delta G_{C\text{-}O}$ in accurately predicting pK_{cycl} values of rhodamines, we employed quantum chemical calculations to predict bright hydroxymethyl rhodamine dyes with proper pK_{cycl} values sitting in the spontaneously blinking window. Besides the requirements of calculated $\Delta G_{C\text{-}O} \in$ [1.156, 1.248 eV], we have outlined two additional design criteria.

1. *Prevention of twisted intramolecular charge transfer (TICT) to enhance quantum yields.* The formation of the TICT state is a major non-radiative decay mechanism that deteriorates the quantum yields of rhodamines.[17] Suppressing TICT formation enhances the quantum yields and improves the overall brightness of fluorophores.[4c,18] This enhancement can be achieved either by reducing the electron-donating strength of the amino group (R; Figure 1a) and/or adjusting steric hindrance.
2. *Incorporation of handles for easy functionalization.* During our computational modeling, a carboxylate acid group has been incorporated in the *meso*-phenyl rings of rhodamines to allow for simple post-synthetic functionalization (by easily adding other linker groups for labeling different subcellular structures). Our calculations showed that these handle groups greatly affect the pK_{cycl} values and the blinking performance of rhodamine dyes and should be considered carefully. For example, the $\Delta G_{C\text{-}O}$ values are 1.191 and 1.267 eV with and without this −COOH handle in **U7**, respectively. Alternatively, this functionalization can also be achieved by extending the hydrocarbon chains of the amino groups (R) in rhodamines, which does not affect the pK_{cycl} values much.

Based on these design criteria and our previous work on tuning the ring-opening tendency of rhodamines,[5] we have computationally designed five potential spontaneously blinking rhodamines of different colors by varying the R and Y substituents (Figures 1a and 2c–e). Calculated $\Delta G_{C\text{-}O}$ ranges from 1.190 to 1.244 eV (Figure 2c; Supporting Information, Figures S40–S44, Table S7); predicted pK_{cycl} values of these rhodamines are within [5.0, 6.3]. It is highly likely that these rhodamines are spontaneously blinking dyes. Notably, our designs incorporate secondary amino groups or (substituted) azetidinyl or quaternary piperazine R groups to suppress TICT formations. We thus expect that these fluorophores possess excellent brightness.

Experimental Synthesis and Characterization of Spontaneously Blinking Rhodamines

To validate our computational designs, we synthesized **RDM1** and **RDM5** following the steps described in the Supporting Information, Figure S45 and Section 5; Figures S46–S62), and studied their spectroscopic properties in various solvents (Figure 3; Supporting Information, Figures S63, S64). In aqueous solution, the UV/Vis absorption spectrum of Si-rhodamine **RDM1** peaked at 655 nm (Figure 3a) along with a maximum fluorescence intensity at 669 nm (Figure 3b). Such near-infrared absorption and emission wavelengths are favorable for bioimaging applications, due to low phototoxicity, deep penetration, and negligible auto-fluorescence from cells and tissues.[19] Moreover, **RDM1** possesses a large brightness ($\varepsilon \times \varphi = 41\,280\ M^{-1}cm^{-1}$) in acidic solution (Figure 3g), which is 21% higher than that of **HMSiR** ($\varepsilon \times \varphi = 34\,100\ M^{-1}cm^{-1}$).[2b] Interestingly, the quantum yield of **RDM1** ($\varphi = 0.32$) is relatively low with respect to that of other azetidine substituted Si-Rhodamine (X = −COO−; $\varphi = 0.54$),[18] which is probably due to different degrees of rotational freedom of the *meso*-phenyl rings as we changed the ring locking groups. Most importantly, pH titration showed that the pK_{cycl} value of **RDM1** is 5.3 (Figure 3a–c), falling into the proposed spontaneously blinking zone.

The UV/Vis and fluorescence wavelengths of **RDM5** (λ_{abs}/λ_{em} = 531/555 nm in aqueous solution) are in the green region (Figure 3d,e). Similarly, **RDM5** demonstrates a significant brightness ($\varepsilon \times \varphi = 65\,250\ M^{-1}cm^{-1}$) in acidic media (Figure 3g), which almost doubles that of conventional dimethy-

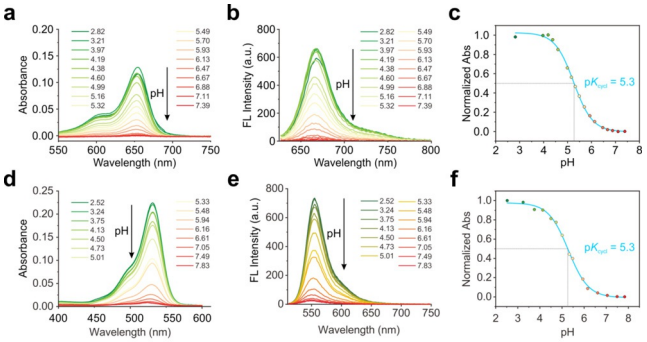

g

Compound	Solvent	λ_{abs} (nm)	λ_{em} (nm)	ε (10^4 $M^{-1}cm^{-1}$)	φ
RDM1	ACN	655	670	10.7	0.49
	$CHCl_3$	657	668	12.7	0.50
	DMSO	667	683	4.4	0.36
	EA	658	675	3.7	0.64
	EtOH	657	689	15.3	0.42
	H_2O	655	669	12.9	0.32
RDM5	ACN	533	558	8.0	0.75
	EA	541	559	1.8	0.95
	EtOH	537	558	3.3	0.68
	H_2O	531	555	8.7	0.75

Figure 3. a) UV/Vis spectra, b) fluorescence spectra, and c) normalized peak UV/Vis absorbance of **RDM1** in the visible region as a function of pH in aqueous solution. d) UV/Vis spectra, e) fluorescence spectra and f) normalized peak UV/Vis absorbance of **RDM5** in the visible region as a function of pH in aqueous solution. g) The photophysical properties of **RDM1** and **RDM5** in various solvents.

lamino substituted rhodamines. Again, experiments showed that the pK_{cycl} value of **RDM5** is 5.3 (Figure 3 f), the same as that of **RDM1**. The measured pK_{cycl} values are close to our computational predictions, corroborating the predictive power of calculated $\Delta G_{C\text{-}O}$. Based on their λ_{abs} values, we named **RDM1** and **RDM5** as **HM-DS655** and **HM-DS531**, respectively.

Evaluation of the Spontaneously Blinking Properties of HM-DS655 and HM-DS531

Inspired by the accurate predictions and successful synthesis of potential spontaneously blinking rhodamine dyes **HM-DS655** (**RMD1**) and **HM-DS531** (**RDM5**), we next studied their single-molecule fluorescent properties (Figure 4). In addition to these two compounds, we also measured **TMSiR** and **TMR** (Figure 4 a,b) as references. **TMSiR** and **TMR** always stay in the open form (fluorescent), and do not undergo spirocyclization reactions.

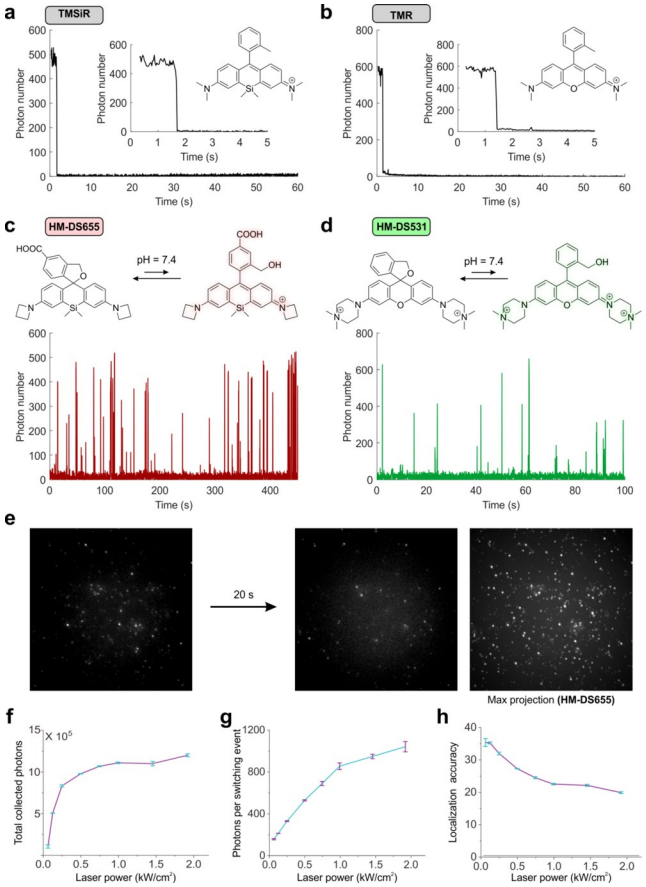

Figure 4. Representative single-molecule fluorescence traces of a) **TMSiR**, b) **TMR**, c) **HM-DS655**, d) **HM-DS531** in PMMA films (excited at 640 nm for **TMSiR** and **HM-DS655** with a laser power of 1.92 kW cm^{-2} and at 561 nm for **TMS** and **HM-DS531** with a laser power of 1.20 kW cm^{-2}), and e) the corresponding max projection image of **HM-DS655**. Single-molecule characteristics of **HM-DS655** under a set of laser power at 640 nm in PBS: f) the total collected photons, g) photons per switching event, h) the localization accuracy as a function of laser power at 0.062, 0.124, 0.496, 0.744, 0.992, 1.456, 1.920 kW cm^{-2}.

We dispersed these compounds in polymethyl methacrylate (PMMA) films at low concentrations. We then collected microscopy images of these compounds, without performing prior photobleaching via intense laser irradiations. As expected, in the absence of spirocyclization reactions, **TMSiR** and **TRM** did not blink much. They continuously emitted, before being photobleached after several seconds of laser irradiations. In contrast, **HM-DS655** and **HM-DS531** underwent many cycles of fluorescence ON/OFF switching due to ground state spirocyclization equilibria for over hundreds of seconds (Figure 4 c–e). Statistical analysis showed that the lifetime in the ON state (the open form) is approximately 90 ms for **HM-DS655** and 50 ms for **HM-DS531** in PMMA films, respectively (Supporting Information, Figures S65–S68).

We also measured the open form lifetime of both **HM-DS655** and **HM-DS531** via laser flash photolysis in PBS. PBS servers as a medium simulating that in live-cell imaging experiments. The measured lifetime amounts to 1.47 ms for **HM-DS531**, and estimated to be on the order of 100 ms for **HM-DS655** (Supporting Information, Figures S69 and S70). These lifetimes (especially that of **HM-DS655**) are compatible with the imaging acquisition speeds of existing detectors.

Finally, we investigated the photon output of **HM-DS655** under various laser powers under bioimaging conditions (Figure 4 f–h; Supporting Information, Figures S71–S81). We attached a SNAP-tag to **HM-DS655**, resulting in the formation of **HM-DS655-SNAP** (Supporting Information, Figure S45). We fixed **HM-DS655-SNAP** to the bottom of a culture dish by linking them to SNAP tags (Supporting Information, Section 2.4.5). Subsequent imaging studies and statistical analysis showed that the total collected photons and photons per switching event increase as the laser power rises, which leads to an improvement in imaging resolution (Figure 4 f,g). A high spatial resolution (ca. 20 nm) is achieved as the laser power increases to about 1 kW cm^{-2} and above (Figure 4 h). Notably, we obtained a good resolution of about 35 nm even when the laser power decreased to 62 W cm^{-2} (Figure 4 h). Accordingly, one may adjust the laser excitation power to achieve the required resolution; long-term imaging could be achieved with low intensity laser irradiations.

Overall, these single-molecule studies provide unambiguous evidence for the spontaneously blinking properties of **HM-DS655** and **HM-DS531** and demonstrate the reliability of $\Delta G_{C\text{-}O}$ based prediction method.

Validation of Super-Resolution Imaging Applications

We applied **HM-DS655-SNAP** to stain mitochondria in fixed HeLa cells, which has been transfected by pSNAPf-Cox8A. In the subsequent 3D-STORM imaging (with ca. 30 000 frames), **HM-DS655-SNAP** demonstrated excellent spontaneously blinking properties and good photostability. This enabled super-resolution imaging of mitochondria with a depth of about 600 nm (Figure 5 a; Supporting Information Figure S82). Our imaging experiments revealed the rich 3D morphologies of mitochondria at nanometer resolution, including branching, linear, clubbed, rotund, and annular

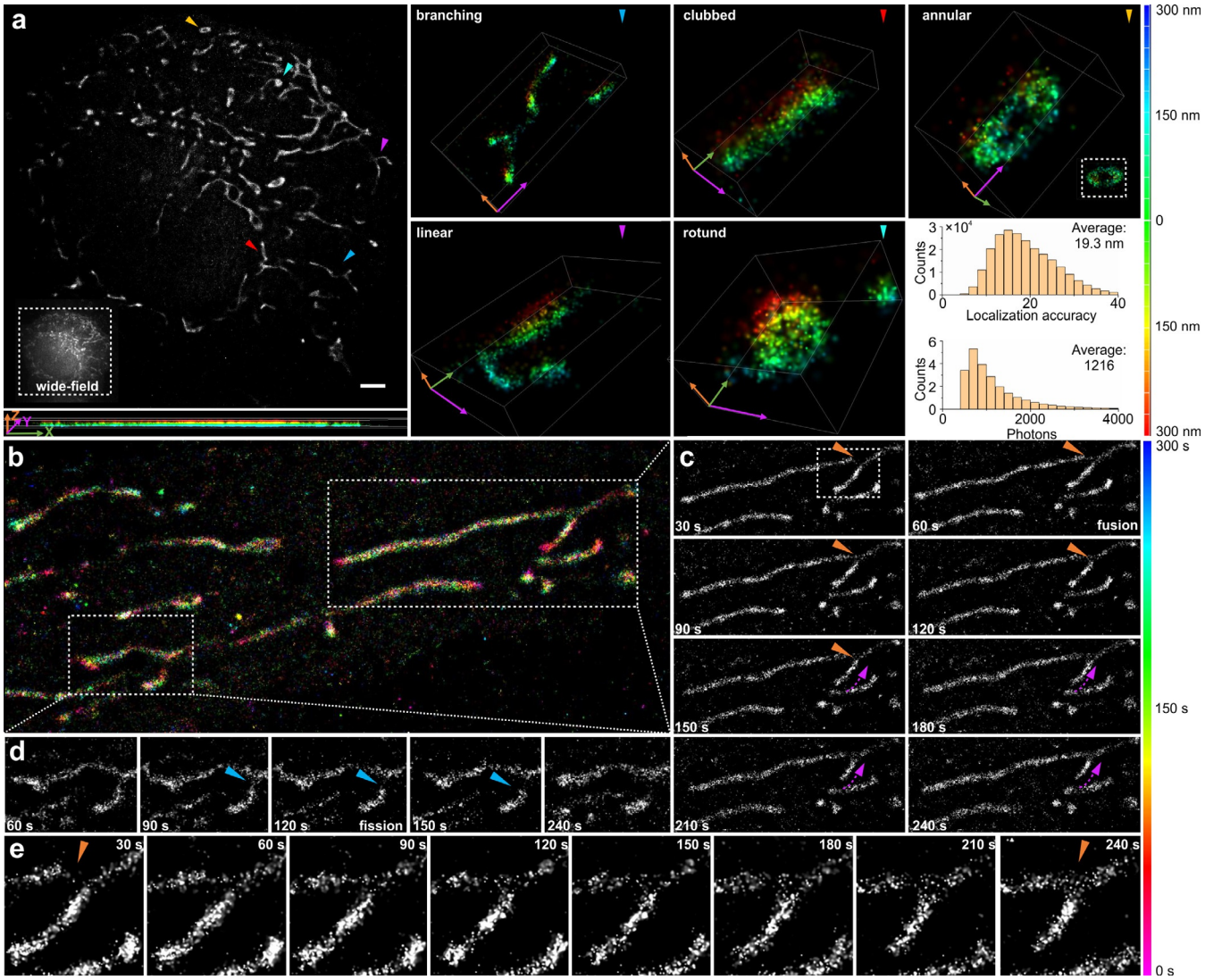

Figure 5. a) 3D-STORM imaging of mitochondria with **HM-DS655-SNAP** in fixed HeLa cells which expressed SNAP-Cox8A. Inset: Wide-field imaging of mitochondria in fixed HeLa cells. Right: 3D view of mitochondria of different shapes, and histograms of localization accuracy and photons per single molecule per frame. b) Overlaid time-lapse images of mitochondria in live HeLa cell. c) Zoom-in view of the fusion process of two mitochondria. d) Zoom-in view of the fission process of two mitochondria. e) Zoom-in view of the fusion process of two mitochondria in (c). Excitation wavelength = 640 nm; excitation power = 1.92 kW cm^{-2}. Scale bar: 2 μm.

structures. The average photon number of a single molecule per frame amounts to 1216, leading to an average optical resolution of 19.3 nm (Figure 5a). Such rich morphologies revealed via super-resolution imaging indicated the dynamic interactions between mitochondria and other organelles.

Inspired by these 3D super-resolution imaging results, we investigated the mitochondria dynamics in live HeLa cells using **HM-DS655-SNAP** (Figure 5b–e; Supporting Information, Figure S83). We reconstructed super-resolution images based on every 1500 frames of raw images. Continuous imaging acquisition further allowed us to construct time-lapse images (Figure 5c–e). In these images, we observed the fusion of two mitochondria as a result of the movements of two branches (highlighted by orange and pink arrows; Figure 5c,e). We also captured the fission of mitochondria (highlighted by blue arrows; Figure 5d).

An ideal fluorophore should label different biomolecules with the attachment of different positioning groups. Accordingly, we verified the ability of **HM-DS655** in labeling and imaging other organelles. We synthesized **HM-DS655-NHS** (Supporting Information, Figure S45) to label the secondary antibody, and then immunostained microtubules in fixed HeLa cells (Figure 6a–c). Once again, **HM-DS655-NHS** demonstrated outstanding spontaneously blinking properties, which allowed the reconstruction of microtubules with an average resolution of 14.1 nm (Figure 6d). In this experiment, the average photon number of a single molecule per frame is 1387 (Figure 6e), similar to that of **HM-DS655-SNAP**.

We also transfected live HeLa cells with SNAP-H2B, and then deployed **HM-DS655-SNAP** to perform 3D-STORM bioimaging of a nucleus. The blinking fluorescent signals enabled us to construct a 3D super-resolution imaging of the

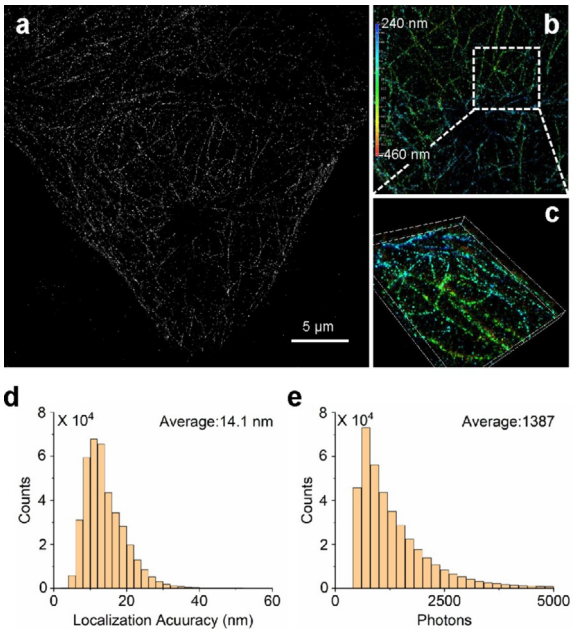

Figure 6. a) 3D-STORM imaging of tubulins in a fixed HeLa with **HM-DS655-NHS**. Scale bar: 5 μm. b),c) 3D view of tubulins. d) Histogram of localization accuracy. e) Histogram of photons per single molecule per frame.

nucleus (Figure 7a–c), with an average photo number per a single molecule per frame of 2545 (Figure 7d), and an average resolution of 25.0 nm (Figure 7e).

Finally, we noted that **HM-DS531** has poor cellular permeability, limiting live-cell bioimaging utilities. However, due to its spontaneously blinking properties, we still successfully deployed **HM-DS531** to image nanostructures formed by block copolymers (Supporting Information, Figure S84).

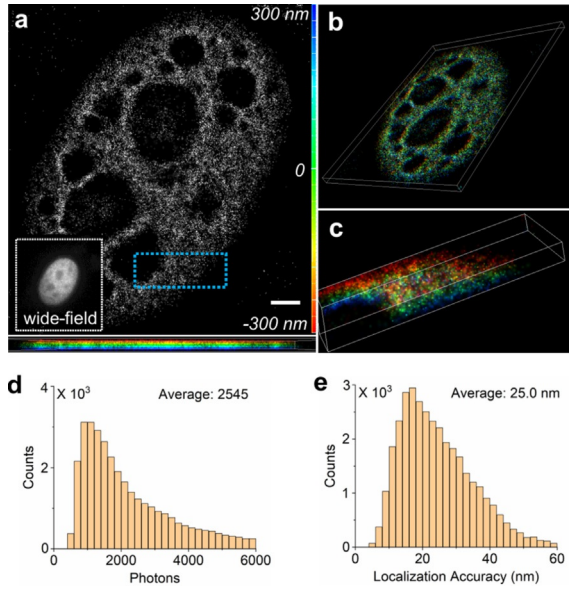

Figure 7. a) 3D-STORM imaging of a nucleus with **HM-DS655-SNAP** in a live HeLa cell which expressed SNAP-H2B. Inset: Wide-field imaging of the nucleus. Scale bar: 2 μm. b) 3D view of the whole nucleus. c) 3D view of ROI in the nucleus. d) Histogram of localization accuracy. e) Histogram of photons per single molecule per frame. Excitation wavelength = 640 nm; excitation power = 1.92 kW cm^{-2}.

Generalization of $\Delta G_{C\text{-}O}$ Based Prediction Model

The $\Delta G_{C\text{-}O}$-pK_{cycl} correlation can also be established in rhodamine derivatives with other X groups. Given that these X groups encounter different environmental interactions (which are not well accounted in existing solvation models), the offset between the calculated and experimental $\Delta G_{C\text{-}O}$ varies as X switches from $-CH_2-O-$ to other ring locking groups (such as X = $-CH_2-NH-$ and $-COO-$). Consequently, slightly different fitting between $\Delta G_{C\text{-}O}$ and pK_{cycl} needs to be established as X changes. Yet, we noted an excellent linear $\Delta G_{C\text{-}O}$-pK_{cycl} correlation ($r^2 = 0.942$) in five aminomethyl rhodamines with X = $-CH_2-NH-$, which were also reported by the Urano group (Figure 8a; Supporting Information, Figures S85, 86, and Table S8).[2b]

Instead of pK_{cycl} values, the population of open ring rhodamines can also be directly quantified via the $K_{L\text{-}Z}$ values (although this is a challenging task when the population of the open form rhodamines becomes small). To this end, the Lavis group has reported the $K_{L\text{-}Z}$ values of 13 ester-rhodamine dyes with X = $-COO-$ (Supporting Information, Figure S87).[12,20] They further proposed that a $K_{L\text{-}Z}$ value between 10^{-2} and 10^{-3} is a good indication of fluorogenic dyes. We hypothesized that a correlation between these experimental $K_{L\text{-}Z}$ values and calculated $\Delta G_{C\text{-}O}$ data might exist. Indeed, subsequent calculations yield a linear $\Delta G_{C\text{-}O}$–log$K_{L\text{-}Z}$ correlation with $r^2 = 0.92$ (Figure 8b; Supporting Information, Figures S88–S100; Table S9).

These correlations could greatly facilitate chemists to design rhodamines with the required pK_{cycl} or $K_{L\text{-}Z}$ values for realizing spontaneous blinking or fluorogenic imaging. To this end, it is worth mentioning that pK_{cycl} $\in$ [5.3, 6.0] only serves as a guideline for developing spontaneously blinking dyes; and this spontaneously blinking window is not rigid. The exact requirements of pK_{cycl} also depend on many other factors. For example, a lower local polarity and a smaller labeling density would tolerate a higher pK_{cycl} value for spontaneously blinking rhodamines, and an acidic environment demands a lower pK_{cycl} value to ensure sparse emissions. Furthermore, changing X may also shift the spontaneously blinking window in consideration of their distinct pH titration curves with different slopes (Supporting Information, Figure S101).

In all these cases, however, the excellent correlation between $\Delta G_{C\text{-}O}$ and pK_{cycl}/$K_{L\text{-}Z}$ (or other parameters reflecting the open form population of rhodamines) offers a convenient tool to aid chemists in the quantitative designs of rhodamines with tailored spirocyclization equilibria.

Conclusion

We have demonstrated a general theoretical descriptor $\Delta G_{C\text{-}O}$, which demonstrates excellent correlations with experimental parameters (such as pK_{cycl} and $K_{L\text{-}Z}$) that reflect

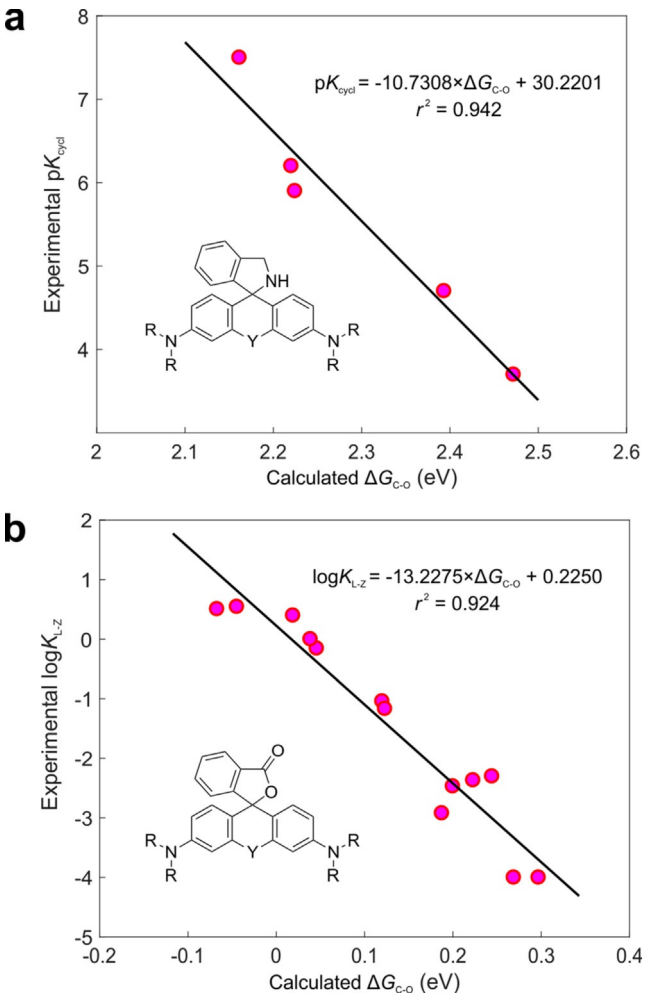

Figure 8. a) Correlation between calculated $\Delta G_{C\text{-}O}$ and experimental pK_{cycl} values for a series of aminomethyl rhodamine dyes reported by the Urano group. b) Correlation between calculated $\Delta G_{C\text{-}O}$ and experimental $K_{L\text{-}Z}$ values for a series of ester-rhodamine dyes reported by the Lavis group. During these calculations, we use zwitterions to represent the open forms.

the open form populations of various rhodamines. Accordingly, $\Delta G_{C\text{-}O}$ allows rapid and quantitative designs of spontaneously blinking rhodamines with different colors, based on simple ground state calculations. The predictive power of $\Delta G_{C\text{-}O}$ has been successfully validated via the synthesis and applications of two novel spontaneously blinking hydroxymethyl rhodamines (**HM-DS531** and **HM-DS655**) with enhanced brightness and outstanding photostability. We have also demonstrated the bioimaging utilities of near-infrared **HM-DS655** for SMLM super-resolution imaging both in vitro and in vivo. Furthermore, we showed that $\Delta G_{C\text{-}O}$ is applicable in predicting the open form populations in a wide range of rhodamines with different ring-locking groups X. Given that the spirocyclization equilibrium of these rhodamine dyes could be fine-tuned by various substitutions at different xanthene positions, we expect that $\Delta G_{C\text{-}O}$ will facilitate chemists to efficiently develop a large number of rhodamines with tailored open form populations, such as multi-colored spontaneously blinking and fluorogenic rhodamines. The availabilities of these high-performance fluorophores will significantly expedite the development and applications of super-resolution imaging techniques in biological research.

Acknowledgements

This work is supported by the National Natural Science Foundation of China (21878286, 21908216), Dalian Institute of Chemical Physics (DMTO201603, TMSR201601), Singapore University of Technology and Design (SUTD) and the SUTD-MIT International Design Centre (IDC) [T1SRCI17126, IDG31800104]. The authors would like to acknowledge the use of the computing service of SUTD-MIT IDC and the National Supercomputing Center (Singapore).

Conflict of interest

The authors declare no conflict of interest.

Keywords: Gibbs free energy · rhodamines · single-molecule localization microscopy · spontaneously blinking dyes · super-resolution imaging

[1] a) Y. Zhang, L. K. Schroeder, M. D. Lessard, P. Kidd, J. Chung, Y. Song, L. Benedetti, Y. Li, J. Ries, J. B. Grimm, L. D. Lavis, P. De Camilli, J. E. Rothman, D. Baddeley, J. Bewersdorf, *Nat. Methods* **2020**, *17*, 225–231; b) M. Sauer, M. Heilemann, *Chem. Rev.* **2017**, *117*, 7478–7509; c) H. Li, J. C. Vaughan, *Chem. Rev.* **2018**, *118*, 9412–9454; d) T. Klein, A. Löschberger, S. Proppert, S. Wolter, S. van de Linde, M. Sauer, *Nat. Methods* **2011**, *8*, 7–9; e) E. Betzig, *Rev. Mod. Phys.* **2015**, *87*, 1153–1168; f) B. Huang, H. Babcock, X. Zhuang, *Cell* **2010**, *143*, 1047–1058; g) P. R. Nicovich, D. M. Owen, K. Gaus, *Nat. Protoc.* **2017**, *12*, 453–460; h) F. Levet, G. Julien, R. Galland, C. Butler, A. Beghin, A. Chazeau, P. Hoess, J. Ries, G. Giannone, J.-B. Sibarita, *Nat. Commun.* **2019**, *10*, 2379; i) H. He, Z. Ye, Y. Zheng, X. Xu, C. Guo, Y. Xiao, W. Yang, X. Qian, Y. Yang, *Chem. Commun.* **2018**, *54*, 2842–2845; j) R. Wombacher, M. Heidbreder, S. van de Linde, M. P. Sheetz, M. Heilemann, V. W. Cornish, M. Sauer, *Nat. Methods* **2010**, *7*, 717–719; k) S. Hauke, A. von Appen, T. Quidwai, J. Ries, R. Wombacher, *Chem. Sci.* **2017**, *8*, 559–566.

[2] a) P. Werther, K. Yserentant, F. Braun, N. Kaltwasser, C. Popp, M. Baalmann, D.-P. Herten, R. Wombacher, *Angew. Chem. Int. Ed.* **2020**, *59*, 804–810; *Angew. Chem.* **2020**, *132*, 814–820; b) S. Uno, M. Kamiya, T. Yoshihara, K. Sugawara, K. Okabe, M. C. Tarhan, H. Fujita, T. Funatsu, Y. Okada, S. Tobita, Y. Urano, *Nat. Chem.* **2014**, *6*, 681–689.

[3] a) L. D. Lavis, R. T. Raines, *ACS Chem. Biol.* **2014**, *9*, 855–866; b) L. Wang, M. S. Frei, A. Salim, K. Johnsson, *J. Am. Chem. Soc.* **2019**, *141*, 2770–2781; c) G. Lukinavičius, K. Johnsson, *Nat. Chem.* **2014**, *6*, 663–664.

[4] a) A. N. Butkevich, G. Y. Mitronova, S. C. Sidenstein, J. L. Klocke, D. Kamin, D. N. H. Meineke, E. D'Este, P.-T. Kraemer, J. G. Danzl, V. N. Belov, S. W. Hell, *Angew. Chem. Int. Ed.* **2016**, *55*, 3290–3294; *Angew. Chem.* **2016**, *128*, 3350–3355; b) L. Wang, M. Tran, E. D'Este, J. Roberti, B. Koch, L. Xue, K. Johnsson, *Nat. Chem.* **2020**, *12*, 165–172; c) Z. Ye, W. Yang, C. Wang, Y. Zheng, W. Chi, X. Liu, Z. Huang, X. Li, Y. Xiao, *J. Am. Chem. Soc.* **2019**, *141*, 14491–14495; d) Q. Qi, W. Chi, Y. Li, Q. Qiao, J. Chen, L. Miao, Y. Zhang, J. Li, W. Ji, T. Xu, X. Liu, J. Yoon, Z. Xu, *Chem. Sci.* **2019**, *10*, 4914–4922.

[5] W. Chi, Q. Qi, R. Lee, Z. Xu, X. Liu, *J. Phys. Chem. C* **2020**, *124*, 3793 – 3801.
[6] a) S. Wäldchen, J. Lehmann, T. Klein, S. van de Linde, M. Sauer, *Sci. Rep.* **2015**, *5*, 15348; b) F. M. Jradi, L. D. Lavis, *ACS Chem. Biol.* **2019**, *14*, 1077 – 1090; c) A. Fürstenberg, M. Heilemann, *Phys. Chem. Chem. Phys.* **2013**, *15*, 14919 – 14930.
[7] a) J. B. Grimm, T. Klein, B. G. Kopek, G. Shtengel, H. F. Hess, M. Sauer, L. D. Lavis, *Angew. Chem. Int. Ed.* **2016**, *55*, 1723 – 1727; *Angew. Chem.* **2016**, *128*, 1755 – 1759; b) J. C. Vaughan, S. Jia, X. Zhuang, *Nat. Methods* **2012**, *9*, 1181 – 1184.
[8] H. Takakura, Y. Zhang, R. S. Erdmann, A. D. Thompson, Y. Lin, B. McNellis, F. Rivera-Molina, S. Uno, M. Kamiya, Y. Urano, J. E. Rothman, J. Bewersdorf, A. Schepartz, D. Toomre, *Nat. Biotechnol.* **2017**, *35*, 773 – 780.
[9] S. Uno, M. Kamiya, A. Morozumi, Y. Urano, *Chem. Commun.* **2018**, *54*, 102 – 105.
[10] A. Morozumi, M. Kamiya, S. Uno, K. Umezawa, R. Kojima, T. Yoshihara, S. Tobita, Y. Urano, *J. Am. Chem. Soc.* **2020**, *142*, 9625 – 9633.
[11] P. J. Macdonald, S. Gayda, R. A. Haack, Q. Ruan, R. J. Himmelsbach, S. Y. Tetin, *Anal. Chem.* **2018**, *90*, 9165 – 9173.
[12] Q. Zheng, A. X. Ayala, I. Chung, A. V. Weigel, A. Ranjan, N. Falco, J. B. Grimm, A. N. Tkachuk, C. Wu, J. Lippincott-Schwartz, R. H. Singer, L. D. Lavis, *ACS Cent. Sci.* **2019**, *5*, 1602 – 1613.
[13] a) M. Kamiya, D. Asanuma, E. Kuranaga, A. Takeishi, M. Sakabe, M. Miura, T. Nagano, Y. Urano, *J. Am. Chem. Soc.* **2011**, *133*, 12960 – 12963; b) M. Sakabe, D. Asanuma, M. Kamiya, R. J. Iwatate, K. Hanaoka, T. Terai, T. Nagano, Y. Urano, *J. Am. Chem. Soc.* **2013**, *135*, 409 – 414.
[14] a) R. J. Iwatate, M. Kamiya, Y. Urano, *Chem. Eur. J.* **2016**, *22*, 1696 – 1703; b) R. J. Iwatate, M. Kamiya, K. Umezawa, H. Kashima, M. Nakadate, R. Kojima, Y. Urano, *Bioconjugate Chem.* **2018**, *29*, 241 – 244; c) Y. Kuriki, M. Kamiya, H. Kubo, T. Komatsu, T. Ueno, R. Tachibana, K. Hayashi, K. Hanaoka, S. Yamashita, T. Ishizawa, N. Kokudo, Y. Urano, *J. Am. Chem. Soc.* **2018**, *140*, 1767 – 1773; d) Y. Koide, R. Kojima, K. Hanaoka, K. Numasawa, T. Komatsu, T. Nagano, H. Kobayashi, Y. Urano, *Commun. Chem.* **2019**, *2*, 94.
[15] a) Y. Zhao, D. G. Truhlar, *Theor. Chem. Acc.* **2008**, *120*, 215 – 241; b) F. Weigend, R. Ahlrichs, *Phys. Chem. Chem. Phys.* **2005**, *7*, 3297 – 3305; c) A. V. Marenich, C. J. Cramer, D. G. Truhlar, *J. Phys. Chem. B* **2009**, *113*, 6378 – 6396.
[16] a) W. Chi, J. Chen, W. Liu, C. Wang, Q. Qi, Q. Qiao, T. M. Tan, K. Xiong, X. Liu, K. Kang, Y.-T. Chang, Z. Xu, X. Liu, *J. Am. Chem. Soc.* **2020**, *142*, 6777 – 6785; b) C. Wang, Q. Qiao, W. Chi, J. Chen, W. Liu, D. Tan, S. McKechnie, D. Lyu, X.-F. Jiang, W. Zhou, N. Xu, Q. Zhang, Z. Xu, X. Liu, *Angew. Chem. Int. Ed.* **2020**, *59*, 10160 – 10172; *Angew. Chem.* **2020**, *132*, 10246 – 10258; c) W. Chi, J. Chen, Q. Qiao, Y. Gao, Z. Xu, X. Liu, *Phys. Chem. Chem. Phys.* **2019**, *21*, 16798 – 16803.
[17] S. Sasaki, G. P. C. Drummen, G. Konishi, *J. Mater. Chem. C* **2016**, *4*, 2731 – 2743.
[18] J. B. Grimm, B. P. English, J. Chen, J. P. Slaughter, Z. Zhang, A. Revyakin, R. Patel, J. J. Macklin, D. Normanno, R. H. Singer, T. Lionnet, L. D. Lavis, *Nat. Methods* **2015**, *12*, 244 – 250.
[19] a) L. Zhou, Q. Wang, Y. Tan, M. J. Lang, H. Sun, X. Liu, *Chem. Eur. J.* **2017**, *23*, 8736 – 8740; b) A. L. Vahrmeijer, M. Hutteman, J. R. van der Vorst, C. J. H. van de Velde, J. V. Frangioni, *Nat. Rev. Clin. Oncol.* **2013**, *10*, 507 – 518.
[20] J. B. Grimm, A. K. Muthusamy, Y. Liang, T. A. Brown, W. C. Lemon, R. Patel, R. Lu, J. J. Macklin, P. J. Keller, N. Ji, L. D. Lavis, *Nat. Methods* **2017**, *14*, 987 – 994.

Manuscript received: July 24, 2020
Accepted manuscript online: August 10, 2020
Version of record online: September 15, 2020

